Microscale superlubricity of graphite under various twist angles

Wen Wang,[1,*] Jian Shen,[1] and Q.-C. He[1,2,†]

[1]*School of Mechanical Engineering, Southwest Jiaotong University, Chengdu 610031, China*

[2]*Université Paris-Est, Laboratoire de Modélisation et Simulations Multi Echelle, UMR 8208, Centre National de la Recherche Scientifique, 5 boulevard Descartes, 77454 Marne-la-Vallée, France*

(Received 30 September 2018; revised manuscript received 10 January 2019; published 7 February 2019)

The relative rotation and translation of graphene and graphite layers lead to remarkable physical and mechanical phenomena. One such phenomenon for graphite corresponds to the ultralow static and dynamic friction between incommensurate graphene layers, referred to as superlubricity. Even though many studies have been dedicated to this promising phenomenon in recent years, an experimental characterization and a quantitative determination of the effect of relative twist angles on microscale superlubricity are still lacking. The present paper investigates the superlubric properties of microscale graphite under different twist angels by shearing graphite with respect to a substrate. Experimentally, it is surprisingly found that the superlubricity of microscale graphite is almost invariant within a wide range of bicrystal twist angles ($6^\circ \leqslant \theta \leqslant 59^\circ$). This result is confirmed by carrying out molecular dynamics simulations. Further, the influences of twist angles and normal load on the incommensurate-to-commensurate transition are revealed. The estimated critical transition angle is less than 0.1 °. These results allow a better understanding of mesoscopic scale superlubricity and extend its application field.

DOI: 10.1103/PhysRevB.99.054103

I. INTRODUCTION

In recent years, intensive efforts have been dedicated towards the research of friction at atomic scale, mainly owing to the development of miniaturized mechanical components reaching their limits when surface-to-volume ratios become so high that friction, wear, and adhesion drastically reduce the reliability and lifetime of devices [1–3]. Hirano and coworkers introduced the term "superlubricity" in the field of nanotribology for the ultralow frictional state of transitional motion and theoretically clarified the atomistic origin of the frictional force intrinsically generated by the molecular interactions between the constituent atoms of surfaces [4–6]. The practical importance of ultralow friction and its relevance to basic scientific questions have motivated studies towards understanding the underlying conditions. Recently, one of the most studied questions in the field of nanotribology has concerned how the frictional force experienced at an atomically flat incommensurate contact interface of microscale and nanoscale changes with various crystal structures, contact areas, and sliding velocities under different measurement environments [7–17].

Up to now, a continuously growing number of experimental and theoretical results have been reported about high sliding velocity, large contact area, and the high normal load superlubric state [18–22]. However, ultralow friction is strongly dependent on relative twist angles: a large friction peak appears every 60 ° due to the commensurate contact. On the other side, due to thermal effects, incommensurate contact transits spontaneously to the commensurate state [23] in order to minimize the potential energy [24,25]. Despite a very large literature on superlubricity, a quantitative understanding and an experimental characterization of the effect of relative twist angles on microscale superlubricity are still lacking. Here, we report direct and accurate experimental measurements of the effect of twist angles on superlubric properties of micrometer atomic flat graphite by exploiting the self-retraction phenomenon in graphite, where a graphite mesa, after being sheared from its *initio* position, retracts spontaneously back to its original position [26].

Microscale graphite mesas with self-retraction phenomena are single-crystalline materials possessing atomically flat and clean interfaces [25]. In this paper, dynamic friction forces (F_f) of micrometer-size graphite mesas under various twist angles are first measured in an elaborately built system. The contact area in this system is more than seven orders of magnitude larger than previous scanning probe-based studies of superlubricity in graphite [27]. We found that superlubricity of microscale graphite is nearly invariant with respect to a wide range of bicrystal twist angles ($6^\circ \leqslant \theta \leqslant 59^\circ$). Together with molecular dynamics (MD) simulations, our results reveal the influences of twist angles and the normal load on the incommensurate-to-commensurate transition. It is found that the influence of twist angles on F_f is effective only within a limited twist angle less than 0.1 ° and that in a large range of angles friction stays almost unchanged. Large normal load can induce lateral deformation and thus cause the local incommensurate-to-commensurate transition.

*wangwen@swjtu.edu.cn

†Qi-Chang.he@u-pem.fr

II. METHODS

A. Sample preparation

The highly oriented pyrolytic graphite (HOPG) is a lamella material with a brick-wall-like polycrystal structure [25,28] in which the in-plane dimensions of grains are of wideness of about a few to tens of micrometers (parallel to the basal plane) while being three orders of magnitude larger than the perpendicular direction (in the [0001] direction) [28,29]. These grains share the same [0001] direction but are randomly oriented with respect to that direction. This implies that the (0001) interfaces (grain boundaries) are planar and pure twist. In our experimental measurements, graphite mesas are prepared using the same technique as that reported in Ref. [26] with edge width of 3 μm and with height of 1 μm on the surface of a large HOPG purchased from Veeco (ZYB grade). Considering the dimensions of the grains, mesas with the height of 1 μm can often come across at least one grain boundary parallel to the sample surface that runs across the entire mesa [28]. Figure 1(a) illustrates the grain boundary between the upper graphite flake (GF2 gray) and the lower graphite flake (GF1 blue). Due to the arbitrary rotation of GF2 relative to GF1 about a common [0001] axis, the twist grain boundaries (interfaces between GF2 and GF1) are in incommensurate contact and GF2 can slide superlubrically over GF1.

B. Experimental setup and force calibration

All friction force measurements of incommensurate graphite were conducted with a home-built system. Figure 1(c) schematically illustrates the experimental setup. A microforce sensor (FT-S100 from FemtoTools, Switzerland) with a force resolution of 5 nN and a bandwidth of up to 8 kHz is fixed to a nanomanipulator (MM3A from Kleindiek, Germany); velocity was controlled by placing the test samples on a rigid plate affixed to a XYZ stage (XP-611 from XMT). The friction force measurements were made by keeping the upper flake GF2 stationary with the force sensor tip pushing on the side edge of the upper flake GF2 (the tip and sample are simply pushed into contact) and the lower flake GF1 moved forward and backward along with the XYZ stage at a constant velocity, $v = 40\,\mathrm{nm/s}$. All the measurements were performed under an optical microscope (Carl Zeiss Axio Scope A1).

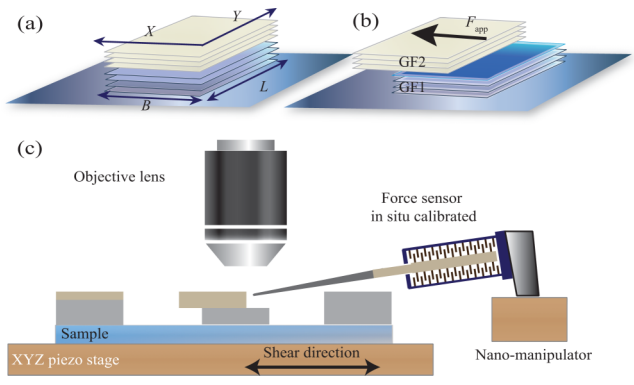

FIG. 1. Experimental setup for F measurement. (a, b) The graphite sample is illustrated as a stack of two thin single-crystalline rectangular graphite flakes, GF1 (blue) and GF2 (gray), with parallel basal planes but with arbitrary twist angles with respect to the common [0001] axis. (b) Schematic illustration of the experimental setup to shear the sample using an XYZ stage. The sample is fixed to a rigid substrate and F_f is measured through shearing GF1 relative to GF2 in the superlubric state.

The force sensor can only measure the force along its axial direction but we focus on the force along the basal plane of mesas, $F = F_S\cos\alpha$, where F_S is the force sensed by the force sensor and α is the angle between the axis of the force sensor and the basal plane of HOPG. In a practical experiment, to obtain more accurate values of F of incommensurate graphite, the microforce sensor needs to be calibrated *in situ*. We carried out this calibration by using a diamagnetic levitation spring system [25,30]. The sensor was recalibrated in each measurement to ensure accuracy in the new round of loading.

III. RESULTS AND DISCUSSION

A. Experimental results

To investigate the frictional characteristics of incommensurate graphite mesa under various twist angels, we focus on the graphite that can self-retract [26] and which has shown high-speed superlubricity at microscale [18,28]. In the practical measurements, we first tested several graphite mesas by a tungsten tip to verify that the self-retracting phenomenon can happen. If the mesas can self-retract, the force and shear displacement of the bottom flake (GF1) are measured during both loading and unloading processes. Figure 2(a) shows a typical force-displacement curve for loading and unloading under ambient conditions (temperature 24 $\pm$ 2 °C, relative humidity 11% $\pm$ 2%) for a square mesa of width $B = 3\,\mu$m and height $H = 1\,\mu$m.

During the loading process, the tip of a force sensor slowly contacts with the side of GF2 where force depends linearly on displacement due to elastic deformation of the microforce sensor. After the applied force exceeds the sum of the retraction and edge force, GF2 starts to move relative to GF1 at a constant velocity (v) and a sudden drop of the force is observed because of the break of edge bonds and adsorptions. After loading a displacement d of about a few hundred nanometers, we unloaded the graphite mesa with the same magnitude of velocity ($-v$) to its initial position. Then, we can obtain the friction force $F_f = \int_0^d (F_L - F_{UL})dx/2d$, where F_L and F_{UL} represent the measured lateral force during the loading and unloading. After GF2 starts to move relative to GF1, both the loading force and unloading force are nearly independent of the displacement [see the region between two vertical dashed lines in Fig. 2(a)], so that we can simply get the friction force by $F_f = (F_L - F_{UL})/2$.

As discussed in previous works on nanoscale graphite [27,31,32], F_f is a function of relative twist angle θ (like grain boundaries in most crystalline materials). Unfortunately, this dependence has not been experimentally determined so far. The next step in determining this twist angle dependence of superlubricity consists in the measurement of the frictional force in terms of θ. This was done based on the lock-in effect [28] referring to the disappearance of self-retraction at a particular twist angle of GF2 relative to GF1 [28]. This can

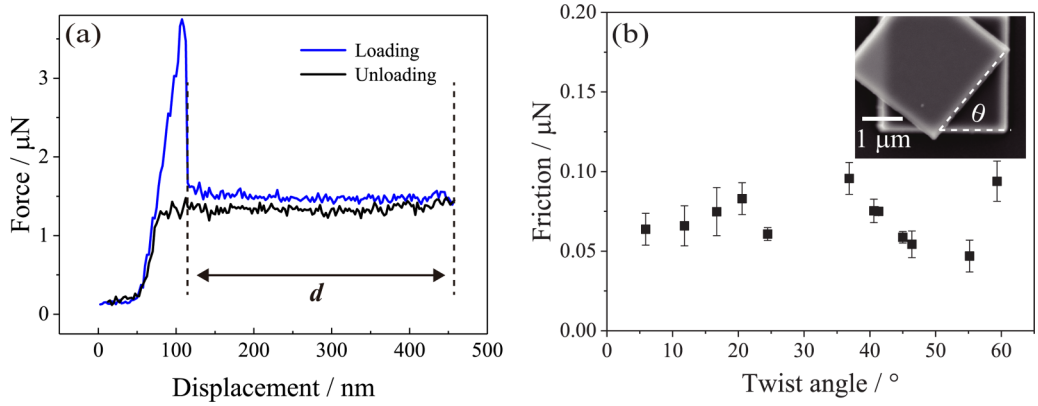

FIG. 2. Results of friction force under various twist angles. (a) Typical force-displacement curves with various temperatures in ambient condition (temperature 24 ± 2 °C, relative humidity 11% ± 2%). The blue lines represent the loading process, and the black lines represent the unloading process. (b) Friction force vs twist angle over the range $6^\circ \leqslant \theta \leqslant 59^\circ$, obtained from 12 samples of the same width $B = 3\,\mu$m and height $H = 1\,\mu$m. The error bars stand for the standard deviation of five independent measurements.

be understood as follows: if two crystals have an arbitrary rotation with respect to one another such that they are in incommensurate contact, the sliding friction is very small [4,6,33]. However, when two graphite flakes are in commensurate contact (perfect ABAB stacking, $\theta = 0$), the barrier to sliding is the theoretical shear strength of the material which is at least three orders of magnitude larger than that for incommensurate contact [28]. By measuring the angle required to rotate GF2 so as to satisfy such a none-retraction condition, we determine the initial rotation of GF2 relative to GF1, i.e., the angle θ. The inset of Fig. 2(b) shows the scanning electron microscopy (SEM) (Quanta FEG 450) image of a flake rotated so as to be aligned along the none-retraction direction and illustrates twist angle measurement.

To investigate the effect of θ on F_f, several experiments were made on different twist angles (temperature 20 ± 2 °C, relative humidity 10% ± 2%). After finishing force measurement, a tungsten tip was used to rotate the sample to obtain none-retraction direction and the above-mentioned method was employed to measure θ. In this manner, and via the precise measurement of the twist angle θ using an SEM, the average dynamic friction of microscale incommensurate graphite is surprisingly found to be nearly independent of twist angle θ. These results [Fig. 2(b)], obtained from 12 samples of the same width $B = 3\,\mu$m and height $H = 1\,\mu$m, hold for the angle range $6^\circ \leqslant \theta \leqslant 59^\circ$. By averaging these data, we obtained an ultralow dynamic friction force per unit area $F_f = 0.008 \pm 0.002$ MPa under atmospheric conditions.

A similar phenomenon was also observed at nanoscale [34]. Previous results obtained by using an atomic force microscopy tip to trigger the motion of a nanoscale graphene layer show that graphene flakes are stable only in commensurate contact related to the substrate graphene layer. Once switched to an incommensurate state, the flakes exhibit facile sliding until another commensurate state is reached. The facile sliding is strongly dependent on relative twist angles: a large friction state appears every 60 ° due to the commensurate contact. However, due to the limit of experimental methods, the size of the sample is restricted to nanoscale and it is difficult to directly measure the friction force at different twist angles. In this paper, we investigate the friction force of microscale graphite under different twist angles by shearing graphite with respect to the substrate.

B. Validations via MD simulations

While several experimental measurements and theoretical predictions were reported for interlayer friction of graphite, little information is available on the twist angle effect and dependence [24,27,31,35,36]. Verhoeven *et al.* [31] theoretically predicted that the full width at half maximum (FWHM) $\Delta\theta$ of the friction peak at nanoscale is simply related to the graphite flake diameter D expressed in lattice spacing by $\tan(\Delta\theta) = \alpha/D$ where the FWHM can be fully recovered with $\alpha = 1$ [37]. Using this simple formula, the estimated value of $\Delta\theta$

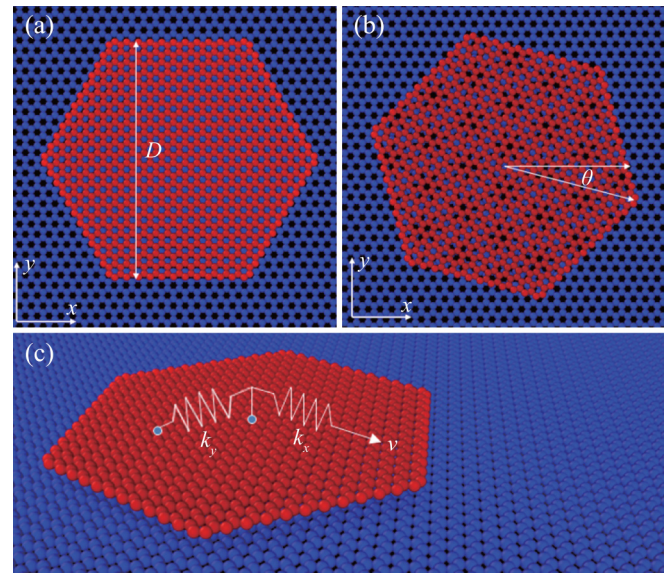

FIG. 3. Atomic model used in the MD simulations. (a) Structure of the hexagonal graphene flake on the two graphene layers in commensurate contact, $\theta = 0^\circ$, and (b) incommensurate contact, $\theta = 15^\circ$. (c) The side view of the three-dimensional MD model with a single layer graphene substrate and a hexagonal graphene flake pulled by a spring with a constant velocity.

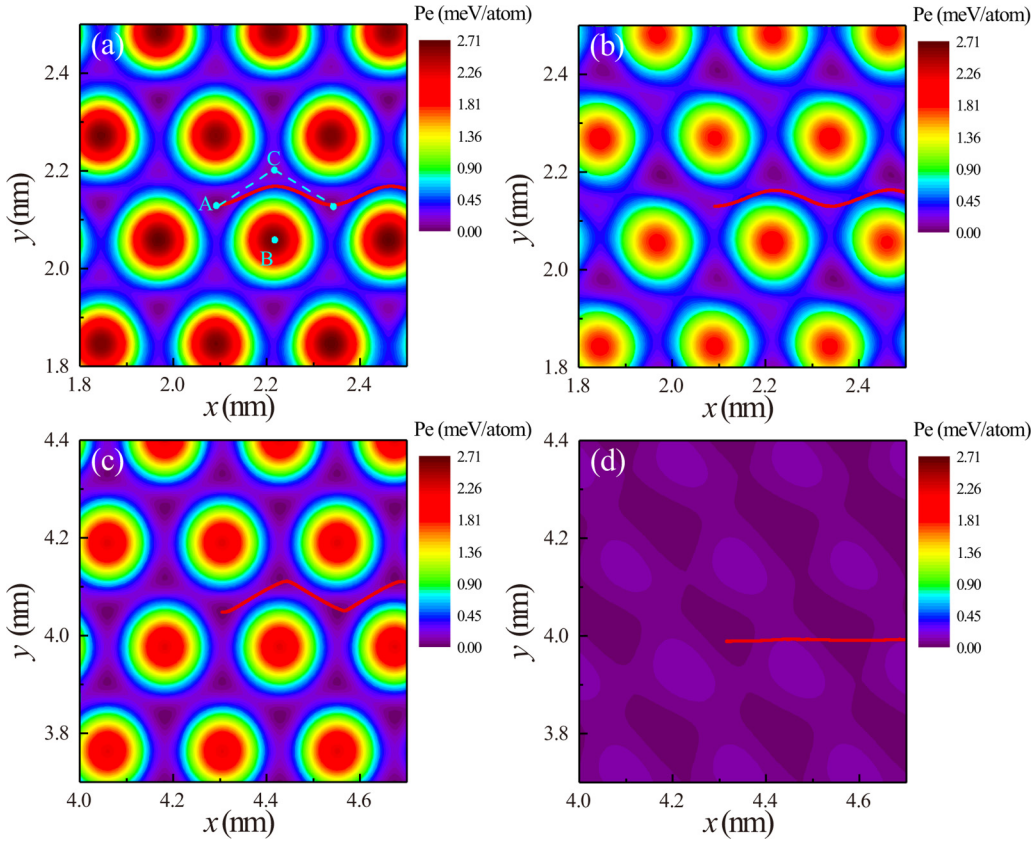

FIG. 4. The effective interaction PES (in eV/atom) between the top graphene flake and the graphene substrate which is given relative to the global energy minimum of the top graphene flake calculated using the Lennard-Jones potential as a function of the position coordinates of the center of mass of the flake, x and y (being the axes chosen along the zigzag and armchair directions, respectively) and in terms of the relative orientation θ (in degrees) under $F_N = 0.2$ nN/atom. (a) $D = 10$ Å, $\theta = 0°$. (b) $D = 10$ Å, $\theta = 6°$. (c) $D = 50$ Å, $\theta = 0°$. (d) $D = 50$ Å, $\theta = 6°$. Red lines correspond to the trajectory of the top graphene flake during sliding.

for microscale superlubricity is less than 0.01 ° and this value is consistent with the results presented in Fig. 2(b).

To validate the experimental results and quantitatively understand both the size effect and normal loads on the incommensurate-to-commensurate transition, we turn to theoretical analysis. In this paper, friction experiments with graphene surfaces are modeled using a MD methodology. Figure 3 illustrates the friction force measuring system used for MD simulations. The MD simulation system consists of single layer fixed square graphene substrate and a layer of hexagonal graphene flake with arbitrary twist angles. The lower layer of graphene is treated as a rigid layer to model the substrate. Figures 3(a) and 3(b) show the atomic model with respective twist angles $\theta = 0°$ (commensurate contact) and 15 ° (incommensurate contact). The twist angle θ is measured relative to the commensurate orientation of the flake so that $\theta = 0°$ and 60 ° are attributed to the commensurate contacting states. All other twist angles correspond to the incommensurate ones. Two linear springs with the spring constant $k_x = k_y = 5.75$ N/m [see Fig. 3(c)] stand for the force sensor that are linked to the top layer of the graphene flake, which consists of atoms moving together, and the atoms of the flake can adjust their relative positions due to deformation [38,39]. Another side of the springs is pulled along the x direction with a constant velocity $v_x = 5$ m/s. The sliding velocities are several orders of magnitude faster than those found in actual experiments due to the limitation of MD timescales.

The in-plane bond interactions between carbon atoms are modeled with reactive empirical bond order (REBO) potential [40], while the interlayer van der Waals interactions are modeled with standard Lennard-Jones 12-6 potential [40] $V_{ij}^{LJ}(r_{ij}) = 4\varepsilon_{ij}[(\frac{\sigma_{ij}}{r_{ij}})^{12} - (\frac{\sigma_{ij}}{r_{ij}})^{6}]$ where ε_{ij} is the bond energy between the carbon atom of the type i and the one of the type j, σ_{ij} is the characteristic length parameter, and r_{ij} is the distance between the two carbon atoms. A cutoff length of 10 Å is used to speed up computations because of the short-range properties of the Lennard-Jones potential. Periodic boundary conditions are imposed to the single layer substrate in both the armchair and zigzag conditions.

Before pulling the top graphene flake, we fist rigidly rotated the top graphene flake to a fixed angle [see Fig. 3(b)]. The distance between the graphene layers was initially set to 0.34 nm and the time step was set to 1 fs for all simulations. To obtain more accurate configuration of the graphene system, the double layer graphene system was first relaxed and equilibrated at constant number, volume, and energy (NVE) ensemble for 80 ps restricting only in-plane rotation of the top graphene flake, and then we applied a normal load F_N to the top graphene flake and equilibrated at the NVE ensemble for 50 ps again. The sign of the normal load is positive when

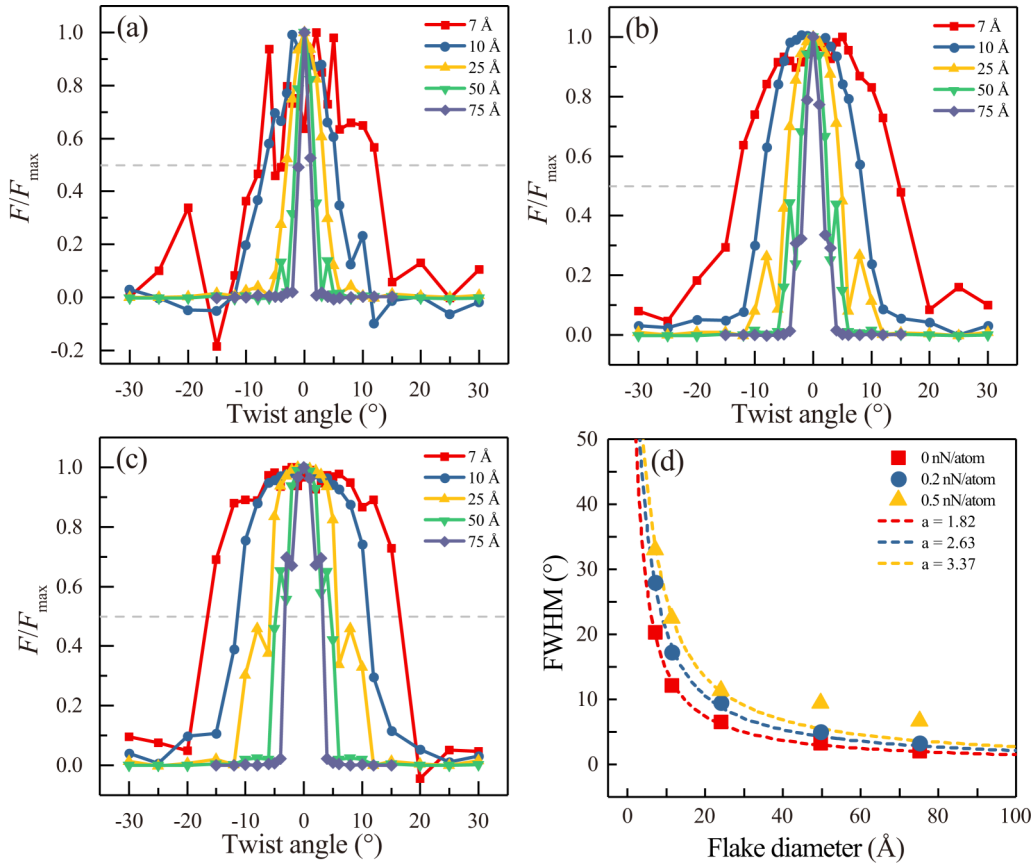

FIG. 5. Size dependence of superlubricity. (a) Normalized friction force as a function of twist angle under normal load $F_N = 0\,\mathrm{nN/atom}$. (b) Normalized friction force under normal load $F_N = 0.2\,\mathrm{nN/atom}$. (c) Normalized friction force under normal load $F_N = 0.5\,\mathrm{nN/atom}$. (d) The calculated FWHM in different normal loads as a function of flake diameters and the theoretical values predicted by Refs. [24,31].

it is compressive. All the simulations were performed at a constant temperature $T = 300\,\mathrm{K}$ with the temperature being controlled by the Langevin thermostats and all the atoms are subjected to the thermostat. The software used for simulation is LAMMPS [38].

To calculate the twist angle dependences of the incommensurate-to-commensurate transition and analyze the possible mechanisms of transition of a graphene flake on graphene layered substrate, it is essential to know the effective interaction potential-energy surface (PES) [41] dependence on twist angles. The interlayer interaction energy (in eV/atom) between the top graphene flake and the graphene substrate is calculated using the Lennard-Jones potential as a function of the position coordinates, x and y, of the center mass of the hexagonal flake (x and y axes are chosen along the zigzag and armchair directions, respectively) and the relative twist angle θ. The calculated potential energy per atom given relative to the global energy minimum of the top graphene flake is shown in Fig. 4 where A and B points represent the PES minima and maxima, respectively. It is clearly indicated from Fig. 4 that PES fluctuations for the twist angle $\theta = 0^\circ$ are much larger than for other orientations, for which the lattices of flake and substrate form a commensurate contact. However, for the same twist angle, the PES fluctuations per atom become smoother with the increase of sample size, which indicates that the critical twist angles needed to realize superlubricity decrease with the increase of sample size. We also drew the trajectory of the top graphene flake in red lines during the sliding where large size sample with commensurate contact shows typical stick-slip curves exhibiting high-energy dissipation [see in Fig. 4(c)]. According to the PES, friction forces can be calculated as $\vec{F_i} = -\nabla_i U = -(\vec{i}\frac{\partial}{\partial x_i} + \vec{j}\frac{\partial}{\partial y_i} + \vec{k}\frac{\partial}{\partial z_i})U$. See Supplemental Material for more information about normal load effects on the effective interaction potential-energy surface [42].

To demonstrate the size-dependent transition, we performed several MD simulations with graphene flake diameter $D = 7$, 10, 25, 50, and 75 Å at the temperature $T = 300\,\mathrm{K}$ by taking the various normal load and twist angles between the graphene flake and substrate. In order to compare friction properties for different size flakes, the friction forces are normalized with respect to the maximal values for each flake. Figures 5(a)–5(c) display the normalized friction force computed as a function of the twist angle under various normal loads. MD results clearly show that the FWHM of friction peaks decreases with the increase of flake diameter under different normal loads and its theoretical values are recovered by various α predicted by Verhoeven *et al.* [31], as can be seen in Fig. 5(d). The results presented here are in agreement with the reported nanoscale experimental data [27,31,32] and previous quasistatic calculations [24,31].

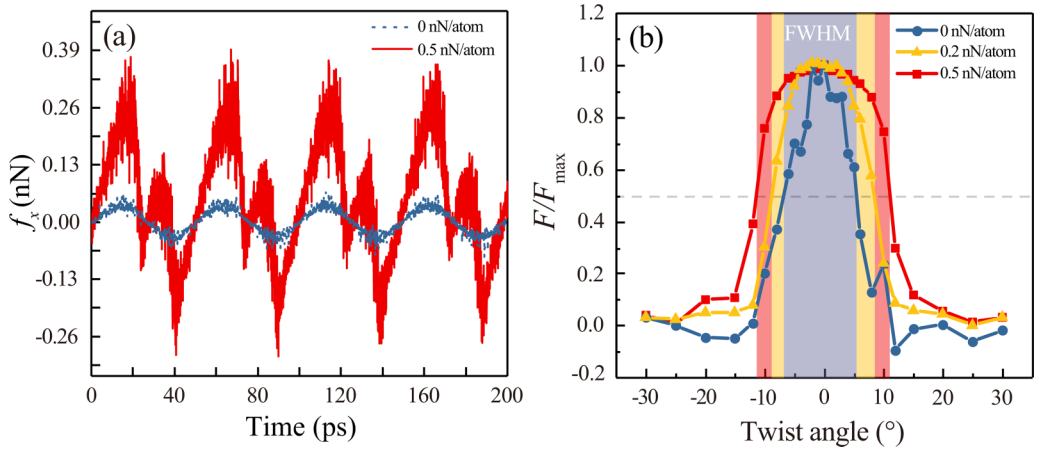

FIG. 6. Normal load dependence of superlubricity. (a) The typical friction force curves experienced by the top graphene flake, showing smooth slide with $D = 10$ Å, $\theta = 0°$, $F_N = 0$ nN/atom and stick-slip with $D = 10$ Å, $\theta = 0°$, $F_N = 0.5$ nN/atom, respectively. (b) The normalized friction force as a function of the twist angle under different normal loads with $D = 10$ Å where the shadow area indicates the calculated FWHM.

According to our results, we can estimate that the critical angle of the incommensurate-to-commensurate transition for microscale samples is less than 0.1 °, which is consistent with our experimental measurements. The thermal fluctuations have an impact on the friction results of small size samples [43,44], especially on the symmetry of the friction force peak. See Supplemental Material for more results at $T = 10$ K [42].

Normal load induces in-plane deformation and thus causes local incommensurate-to-commensurate transition. To investigate the behavior of the transition with normal load, we performed MD simulations at the temperature $T = 300$ K by fixing the graphene flake diameter $D = 10$ Å and by varying normal load to $F_N = 0$, 0.2, and 0.5 nN/atom. Figure 6(a) shows the typical friction force curves experienced by the graphene flake under different normal loads. The increase of normal load leads to the transition from smooth sliding to stick-slip sliding caused by elastic instability. Figure 6(b) shows the results of different normal loads' effects on FWHM and demonstrates three distinct features: (i) commensurate contact can be maintained even at large twist angles by increasing normal load; (ii) for small normal load, commensurate contact transits to incommensurate contact continuously, while for large normal load commensurate contact first transits to local incommensurate contact and then whole incommensurate contact with the increase of twist angle; (iii) increasing the normal load could reduce the thermal fluctuations and also improve the symmetry of typical friction force. These phenomena are caused by in-plane deformation induced by normal load. See Supplemental Material for more discussions about the in-plane deformation [42].

IV. CONCLUSION

In recent years, the most studied question in the field of superlubricity concerns how the frictional force changes with various crystal structures [45,46], sliding directions [36], and contact size [17]. One of the main factors limiting the real application of superlubricity is its strong dependence on relative twist angles: a large friction peak appears every 60 ° due to commensurate contact. Despite a recent abundant literature on superlubricity, the effect of relative twist angles on microscale superlubricity has been far from being experimentally characterized and quantitatively determined. In this paper, we have experimentally measured and numerically simulated the dynamic friction force of incommensurate graphite with various twist angles in ambient laboratory conditions. The experiments and MD simulations carried out have shown that the superlubricity of microscale graphite is nearly invariant when the bicrystal twist angle θ is such that $6° \leqslant \theta \leqslant 59°$. In addition, the influences of the twist angle and the normal load on the incommensurate-to-commensurate transition have been revealed. In particular, the critical angle for the failure of microscale superlubricity is estimated as less than 0.1 °. These results extend the current understanding of superlubricity and are believed to have wide applications, in particular, in microscale devices.

ACKNOWLEDGMENTS

This work was supported by the National Natural Science Foundation of China (Grants No. 11602205, No. 11890672, and No. 11572266) and the Fundamental Research Funds for the Central Universities (Grants No. 2682018CX11 and No. 2682016ZY03).

[1] W. Merlijn van Spengen, Microelectron. Reliab. **43**, 1049 (2003).
[2] S. H. Kim, D. B. Asay, and M. T. Dugger, Nano Today **2**, 22 (2007).
[3] J. A. Williams and H. R. Le, J. Phys. D **39**, R201 (2006).
[4] M. Hirano and K. Shinjo, Phys. Rev. B **41**, 11837 (1990).
[5] M. Hirano, K. Shinjo, R. Kaneko, and Y. Murata, Phys. Rev. Lett. **67**, 2642 (1991).

[6] K. Shinjo and M. Hirano, Surf. Sci. **283**, 473 (1993).
[7] L. Yang, Y. Guo, and Q. Zhang, Diam. Relat. Mater. **73**, 273 (2017).
[8] Q. Xu, X. Li, J. Zhang, Y. Hu, H. Wang, and T. Ma, ACS Appl. Mater. Interfaces **9**, 40959 (2017).
[9] L. Wang, X. Zhou, T. Ma, D. Liu, L. Gao, X. Li, J. Zhang, Y. Hu, H. Wang, Y. Dai, and J. Luo, Nanoscale **9**, 10846 (2017).
[10] P. E. Sheehan and C. M. Lieber, Nano Lett. **17**, 4116 (2017).
[11] A. Özoğul, S. İpek, E. Durgun, and M. Z. Baykara, Appl. Phys. Lett. **111**, 211602 (2017).
[12] D. Mandelli, I. Leven, O. Hod, and M. Urbakh, Sci. Rep. **7**, 10851 (2017).
[13] T. Maeda and H. Washizu, Microsyst. Technol. **24**, 757 (2017).
[14] H. Li, J. Wang, S. Gao, Q. Chen, L. Peng, K. Liu, and X. Wei, Adv. Mater. **29**, 1701474 (2017).
[15] Y. Kobayashi, T. Taniguchi, K. Watanabe, Y. Maniwa, and Y. Miyata, Appl. Phys. Express **10**, 045201 (2017).
[16] Z. Gong, X. Jia, W. Ma, B. Zhang, and J. Zhang, Appl. Surf. Sci. **413**, 381 (2017).
[17] D. Dietzel, J. Brndiar, I. Stich, and A. Schirmeisen, ACS Nano **11**, 7642 (2017).
[18] J. Yang, Z. Liu, F. Grey, Z. Xu, X. Li, Y. Liu, M. Urbakh, Y. Cheng, and Q. Zheng, Phys. Rev. Lett. **110**, 255504 (2013).
[19] R. Zhang, Z. Ning, Z. Xu, Y. Zhang, H. Xie, F. Ding, Q. Chen, Q. Zhang, W. Qian, Y. Cui, and F. Wei, Nano Lett. **16**, 1367 (2016).
[20] R. Zhang, Z. Ning, Y. Zhang, Q. Zheng, Q. Chen, H. Xie, Q. Zhang, W. Qian, and F. Wei, Nat. Nanotechnol. **8**, 912 (2013).
[21] D. Berman, S. A. Deshmukh, S. K. Sankaranarayanan, A. Erdemir, and A. V. Sumant, Science **348**, 1118 (2015).
[22] S. W. Liu, H. P. Wang, Q. Xu, T. B. Ma, G. Yu, C. Zhang, D. Geng, Z. Yu, S. Zhang, W. Wang, Y. Z. Hu, H. Wang, and J. Luo, Nat. Commun. **8**, 14029 (2017).
[23] D. Wang, G. Chen, C. Li, M. Cheng, W. Yang, S. Wu, G. Xie, J. Zhang, J. Zhao, X. Lu, P. Chen, G. Wang, J. Meng, J. Tang, R. Yang, C. He, D. Liu, D. Shi, K. Watanabe, T. Taniguchi, J. Feng, Y. Zhang, and G. Zhang, Phys. Rev. Lett. **116**, 126101 (2016).
[24] A. E. Filippov, M. Dienwiebel, J. W. M. Frenken, J. Klafter, and M. Urbakh, Phys. Rev. Lett. **100**, 046102 (2008).
[25] W. Wang, S. Dai, X. Li, J. Yang, D. J. Srolovitz, and Q. Zheng, Nat. Commun. **6**, 7853 (2015).
[26] Q. Zheng, B. Jiang, S. Liu, Y. Weng, L. Lu, Q. Xue, J. Zhu, Q. Jiang, S. Wang, and L. Peng, Phys. Rev. Lett. **100**, 067205 (2008).
[27] M. Dienwiebel, G. S. Verhoeven, N. Pradeep, J. W. M. Frenken, J. A. Heimberg, and H. W. Zandbergen, Phys. Rev. Lett. **92**, 126101 (2004).
[28] Z. Liu, J. Yang, F. Grey, J. Z. Liu, Y. Liu, Y. Wang, Y. Yang, Y. Cheng, and Q. Zheng, Phys. Rev. Lett. **108**, 205503 (2012).
[29] S. Park, H. C. Floresca, Y. Suh, and M. J. Kim, Carbon **48**, 797 (2010).
[30] Q. Li, K. S. Kim, and A. Rydberg, Rev. Sci. Instrum. **77**, 065105 (2006).
[31] G. S. Verhoeven, M. Dienwiebel, and J. W. M. Frenken, Phys. Rev. B **70**, 165418 (2004).
[32] M. Dienwiebel, N. Pradeep, G. S. Verhoeven, H. W. Zandbergen, and J. W. M. Frenken, Surf. Sci. **576**, 197 (2005).
[33] M. R. Sorensen, K. W. Jacobsen, and P. Stoltze, Phys. Rev. B **53**, 2101 (1996).
[34] X. Feng, S. Kwon, J. Y. Park, and M. Salmeron, ACS Nano **7**, 1718 (2013).
[35] E. Koren and U. Duerig, Phys. Rev. B **93**, 201404(R) (2016).
[36] E. Gnecco, Europhys. Lett. **91**, 66008 (2010).
[37] O. Hod, Phys. Rev. B **86**, 075444 (2012).
[38] S. Plimpton, J. Comput. Phys. **117**, 1 (1995).
[39] L. Xu, T.-B. Ma, Y.-Z. Hu, and H. Wang, Nanotechnology **22**, 285708 (2011).
[40] S. J. Stuart, A. B. Tutein, and J. A. Harrison, J. Chem. Phys. **112**, 6472 (2000).
[41] M. Reguzzoni, A. Fasolino, E. Molinari, and M. C. Righi, J. Phys. Chem. C **116**, 21104 (2012).
[42] See Supplemental Material at http://link.aps.org/supplemental/10.1103/PhysRevB.99.054103 for additional theoretical analysis.
[43] L. Prandtl, Z. Angew. Math. Mech. **8**, 85 (1928).
[44] G. Tomlinson, London, Edinburgh Dublin Philos. Mag. J. Sci. **7**, 905 (1929).
[45] I. Leven, D. Krepel, O. Shemesh, and O. Hod, J. Phys. Chem. Lett. **4**, 115 (2012).
[46] H. Zhang, Z. Guo, H. Gao, and T. Chang, Carbon **94**, 60 (2015).